Online Supplement

Intrinsic adrenal TASK channel dysfunction produces spontaneous calcium oscillations sufficient to drive angiotensin II-resistant hyperaldosteronism.

Christina A. Gancayco[1], Molly R. Gerding[2], David T. Breault[3], Mark P. Beenhakker[2], Paula Q Barrett[2], Nick A. Guagliardo[2]

[1] Medicine-Research Computing and **[2]**Department of Pharmacology, University of Virginia, Charlottesville, VA, USA

[3] Division of Endocrinology, Boston Children's Hospital, Boston, MA, USA and Harvard Stem Cell Institute, Cambridge, MA, USA

Short Title: Spontaneous oscillations drive aldosterone autonomy

Corresponding author:
Nick A. Guagliardo, Ph.D.
University of Virginia
Department of Pharmacology
1340 Jefferson Park Ave
Charlottesville, VA 22908-0735, USA
Phone: 434-924-5644
Email: Nag4g@virginia.edu

Detailed Methods

Adrenal slice preparation.

Adrenals were harvested from deeply anesthetized mice (ketamine 10-15 mg, i.p.), isolated from surrounding fat tissue, and embedded in 3.2% agar/PIPES buffer. Adrenals were sectioned on a vibratome (60–70 µm slices, Microslicer Zero-1, Ted Pella) in ice-cold PIPES incubation buffer (in mM: 20 PIPES, 117 NaCl, 3 KCl, 1 $CaCl_2$, 1 $MgCl_2$, 25 D-Glucose, 5 $NaHCO_3$, pH 7.3 [adjusted with 10N NaOH]), and kept at 37 °C for 25 min. *For calcium imaging experiments:* adrenal slices were then maintained at room temperature in PIPES incubation buffer until time of imaging. Imaging experiments were subsequently carried out in PIPES imaging buffer (see *Calcium Imaging* below). *For Aldosterone secretion experiments:* slices were transferred to cell culture inserts with hydrophilic polytetrafluoroethylene membranes (Millicell, PICM03050) in a six-well plate (Corning, Costar 3513). Slices were laid flat on the insert membrane, 2-3 slices per insert, and placed in a well containing 900ul of secretion media: DMEM/Nutrient mixture F-12 Ham powder (Millipore Sigma, D9785) supplemented with 0.1% BSA, 2.5% Nu-Serum™ IV (Corning, 355104), 200 L-alanyl-L-glutamine dipeptide (GlutaMAX™, Gibco, 35050-061), 1x Insulin-Transferrin-Selenium (Gibco, 41400-045) and adjusted to final concentrations, in mM, 13.5 HEPES, 13.5 NaHCO3, 4 KCl, 2 $CaCl_2$, 110 NaCl, 0.6 $MgCl_2$, 0.4 $MgSO_4$, 16.5 D-Glucose, pH 7.3 (adjusted with 10N NaOH), 280mOsm. For the duration of the experiment, slices were incubated at 37°C with 5% CO_2.

Calcium Imaging.

Adrenal slices were imaged as previously described[1]. Briefly, slices were imaged on a Zeiss Axio-Examiner microscope with X-Cite XLED light source with a 63x immersion objective. Images were acquired continuously at 20 Hz for 10 minutes with a sCMOS camera (Hamamatsu Orca-Flash 4.0) using Slidebook 6 software (Intelligent Imaging Innovations). Adrenal slices were perfused with PIPES imaging buffer (in mM: 20 PIPES, 119 NaCl, 4 KCl, 2 $CaCl_2$, 1 $MgCl_2$, 25 D-Glucose, pH 7.3 [adjusted with 10N NaOH]) and secured using a friction-fit nylon harp that minimized tissue movement. For AngII experiments, AngII (Bachem, H-1705) was added to bath perfusion after 1.5 min of baseline acquisition. In some experiments, slices were pretreated in 200nM A1899 (Tocris, 6972) and 200nM PK-THPP (Tocris, 5338) for 10 min before acquisition. Image sequences were saved as high quality multipage TIFF files for analysis.

Analysis of Calcium Activity.

Spikes: Fluorescent intensity data was extracted and analyzed from acquired images as previously described[1]. Briefly, we used Caltracer software (Yuste lab, Columbia U., Matlab) to designate ROI's overlaying active cells to generate intensity/per ROI/per frame. Experimenter was blind to conditions when selecting ROIs. ROI intensity data from a single experiment were concatenated and events were detected based on peak intensities using custom Matlab script, and were subsequently corrected manually for false events detected, as well as actual events missed by the algorithm. Calcium events are binned into time segments (e.g., 1-min bins) and averaged across cells to establish slice behavior.

Spike Bursts: We defined a calcium burst as 3 or more sequential calcium spikes, with each succeeding spike occurring within the calculated time threshold (Figure 1S) from the previous spike. The identification of discrete bursts of calcium spikes enabled an analysis of zG cell burst properties (e.g., duration, spike frequency, number); we averaged such properties across individual cells to derive a mean value per slice.

Functional Clustering Algorithm: A functional clustering algorithm (described in Feldt et. al.[2]) was used to analyze calcium event patterns among cells, independent of ROI location; i.e., without *a priori* knowledge of cell-cell proximity. Cells that had greater temporal relationships among events present in clusters, graphically represented as groups in a dendrogram. Statistical significance of detected clusters is determined by comparisons to surrogate data sets, and pairing.

zG cell pair-wise distance: Defining the boundary of a rosette based on GCaMP3 fluorescence, and by extension, cell membership to a specific rosette, is a biased determination. To measure proximity of cell-pairs independent of rosette assignment, the distance between the center coordinate of each ROI was extrapolated, and compared between cell-pairs that were members of same cluster (within-cluster) and those that were not (between-clusters).

Phase difference: A second, independent measure of cell-cell calcium events relies on the analysis of time-locked behavior between cell pairs wherein temporal relationships among active zG cells are measured in terms of phase. As previously reported[1], to perform this paired analysis, we determine the timing of each calcium spike in the spike train of one zG cell (test cell) and compared that to the periodic spiking of a second reference cell to obtain a phase-difference. The Standard deviation (SD) of the phase differences between two active cells is a measure of activity interdependence, where a small SD indicates that two cells (cell-pair) are phase-locked with coupled activity (i.e., have a fixed temporal relationship; 0-360º phase difference), while a large SD indicates a random distribution of phase differences (i.e., non-fixed temporal relationship) and thus their activities are uncoupled.

Data are plotted as color-coded matrix plots that reveal phase relationships. In each matrix plot, cell designations (i.e., cell 1, cell 2, etc.) are distributed on both the x and y axis. The phase relationship between the cell on the x-axis and the cell on the y-axis is represented by the color-coded block where they intersect. This color-spectrum corresponds to a continuum of SD values, specified to the right of the matrix plot, from blue (low SD of phase differences, phase-locked) to red (high SD of phase differences, no phase-relationship). Note, cell assignments are arbitrary, and can be distributed on each axis in any order. Because we were asking if phase relationships of within-rosettes cell-pairs differed from between-rosette cell-pairs, we ordered cells on the x and y axis by rosette assignment. Rosette assignment for each cell was determined independently by 2 researchers' best estimation from a z-projection of mean pixel intensity for each adrenal slice.

Aldosterone Secretion.

After a 2-hour equilibration period, slices were transferred to a new well for 30 min (baseline period), and then transferred to wells containing either 0- (control), 50-, 100-, 300-, 1000- pM AngII, or TASK inhibitors (200 nM A1899 + 200nM PK-THPP) for an additional 30 min (drug-treatment period). Aldosterone concentration per well was measured by radioimmunoassay (RIA, Tecan US, Inc., MG13051) and presented as aldosterone (pg)/slice/hour. Total aldosterone secreted per slice is an imperfect measure, given the aggregate of functional zG

cells in any given slice was unknown. Therefore, we implemented a second method of analysis in which each well served as its own control, by calculating the fold change in aldosterone production after drug treatment for each well. For each mouse, the mean ratio of its control slices (vehicle/baseline) was used to standardize all ratios.

Statistics.

Hypotheses were tested for differences in group means of pooled data using a linear mixed model that accounts for the potential within-subject correlation of pseudoreplicates. Both the number of pseudoreplicates (i.e., cells/bursts/pairs/wells) and genuine replicates (i.e., mice) of the multi-level analysis are reported in each figure legend where applicable. For calcium imaging experiments, in which each mouse contributed exactly 1 slice per experimental condition, the slice is considered a true replicate, and each cell (or cell pair) within that slice a pseudoreplicate. Thus correlated error was modeled using a hierarchical structure, with mouse > slice > cell. Similarly, for aldosterone secretion experiments in which each well contained 2-3 adrenal slices from a single mouse, data was modeled using a hierarchy of mouse (replicates) > well (pseudoreplicates).

References:

1. Guagliardo NA, Klein PM, Gancayco CA, Lu A, Leng S, Makarem RR, Cho C, Rusin CG, Breault DT, Barrett PQ, et al. Angiotensin II induces coordinated calcium bursts in aldosterone-producing adrenal rosettes. *Nat Commun*. 2020;11:1679. doi: 10.1038/s41467-020-15408-4
2. Feldt S, Waddell J, Hetrick VL, Berke JD, Zochowski M. Functional clustering algorithm for the analysis of dynamic network data. *Phys Rev E Stat Nonlin Soft Matter Phys*. 2009;79:056104. doi: 10.1103/PhysRevE.79.056104

Supplemental Figures

Figure 1S.

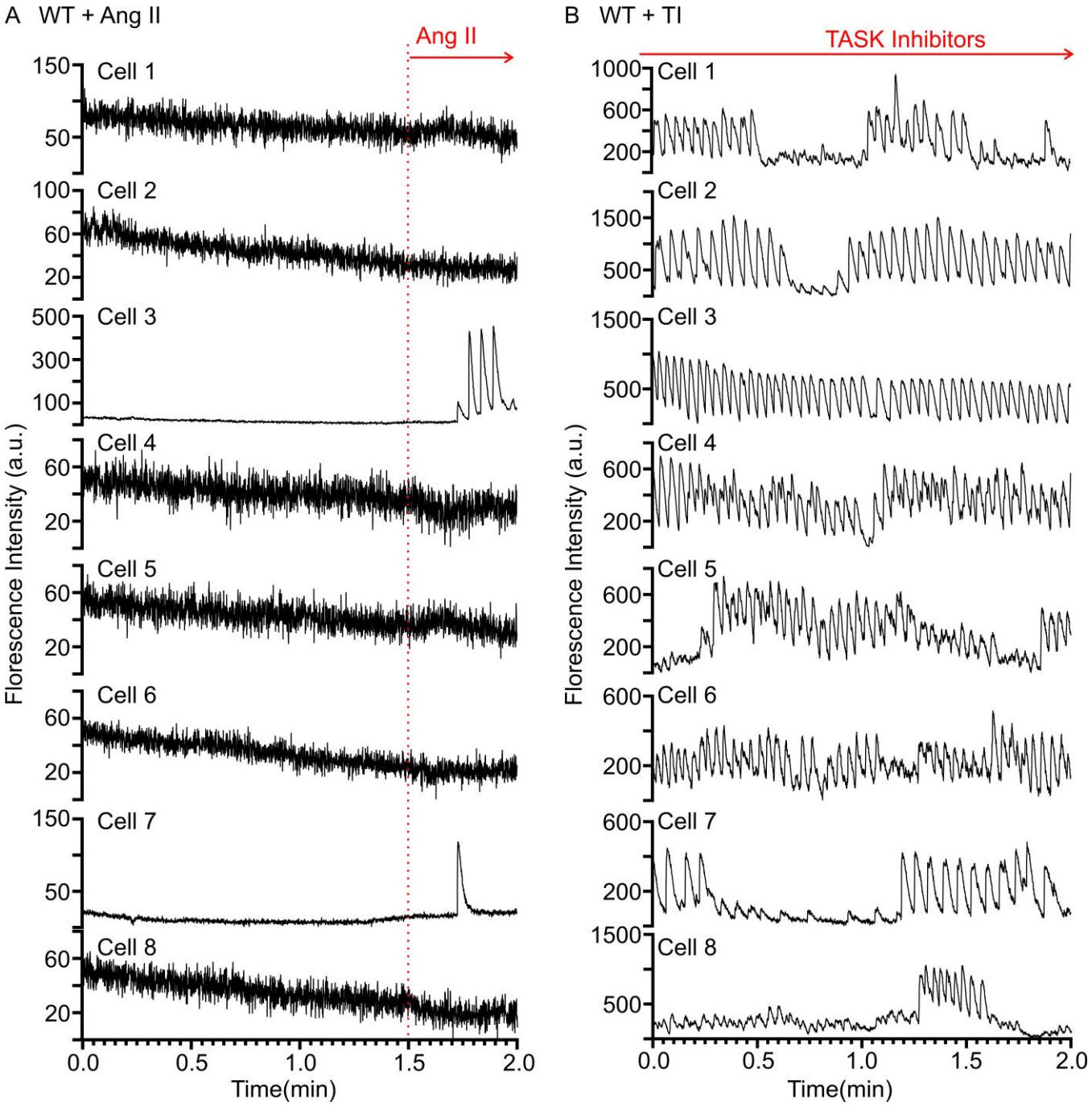

Representative traces of baseline calcium activity in zG cells from WT adrenal slices. GCaMP3 florescent intensity plotted over the first 2 min (sampled at 20 Hz) from WT zG cells either presented with 3nM AngII (red line) after 1.5 min (**A**) or pretreated (10 min) with TASK-1 and TASK-3 inhibitors (**B**,200nM A1899 and 200nM PK-THPP). For illustration purposes, the fluorescent intensity values (a.u.) for each trace were transformed by subtracting that trace's minimum intensity value over the 2 min acquisition period, thus "zeroing" the y-axis.

Figure S2.

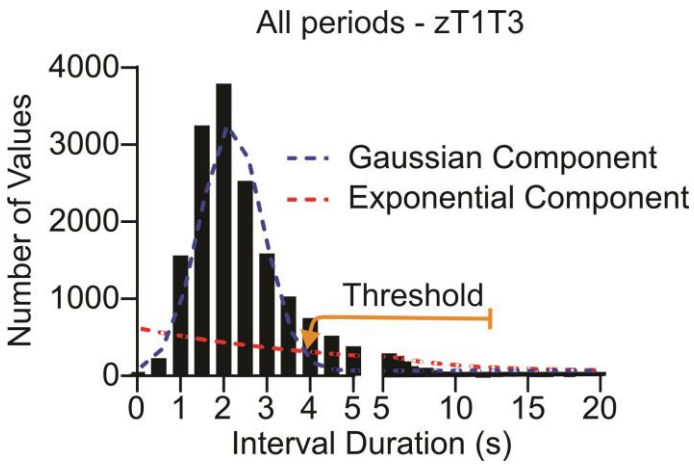

Determining a threshold value for defining a burst of calcium spikes. Threshold (s) for the maximum intra-burst interval within a burst is defined as the intersection of a Gaussian (blue dashed-line) and exponential (red dashed-line) fit to the distribution of inter-spike intervals (black bars). Thus, a burst was determined to begin when the inter-spike interval of 3 or more consecutive spikes was less than the threshold value, and to end when a spike interval in the series was greater than the threshold value.

Figure S3.

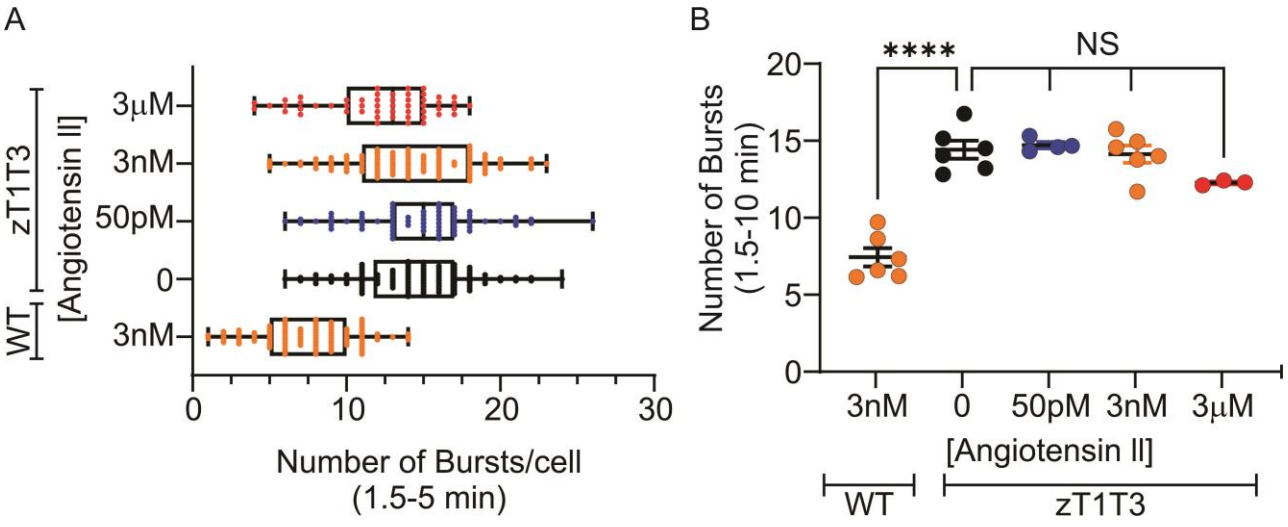

Calcium bursts after AngII stimulation. Expanded data-set presented in Figure 2 to include the entire period of image acquisition after AngII was presented (1.5 -10 min). **A,** the distribution of burst number per cell in WT and zG-TASK-LOF (zT1T3) slices with 0-3 µM AngII added to perfusion bath 1.5 min after the start of image acquisition. Data presented as box and whiskers plot of median (center line) and 25-75 percentiles (box) of distributions. **B**, Corresponding mean burst number/cell/mouse ± SEM. ****P<0.001 as determined by mixed model ANOVA with Bonferroni's multiple comparisons test.

Figure S4.

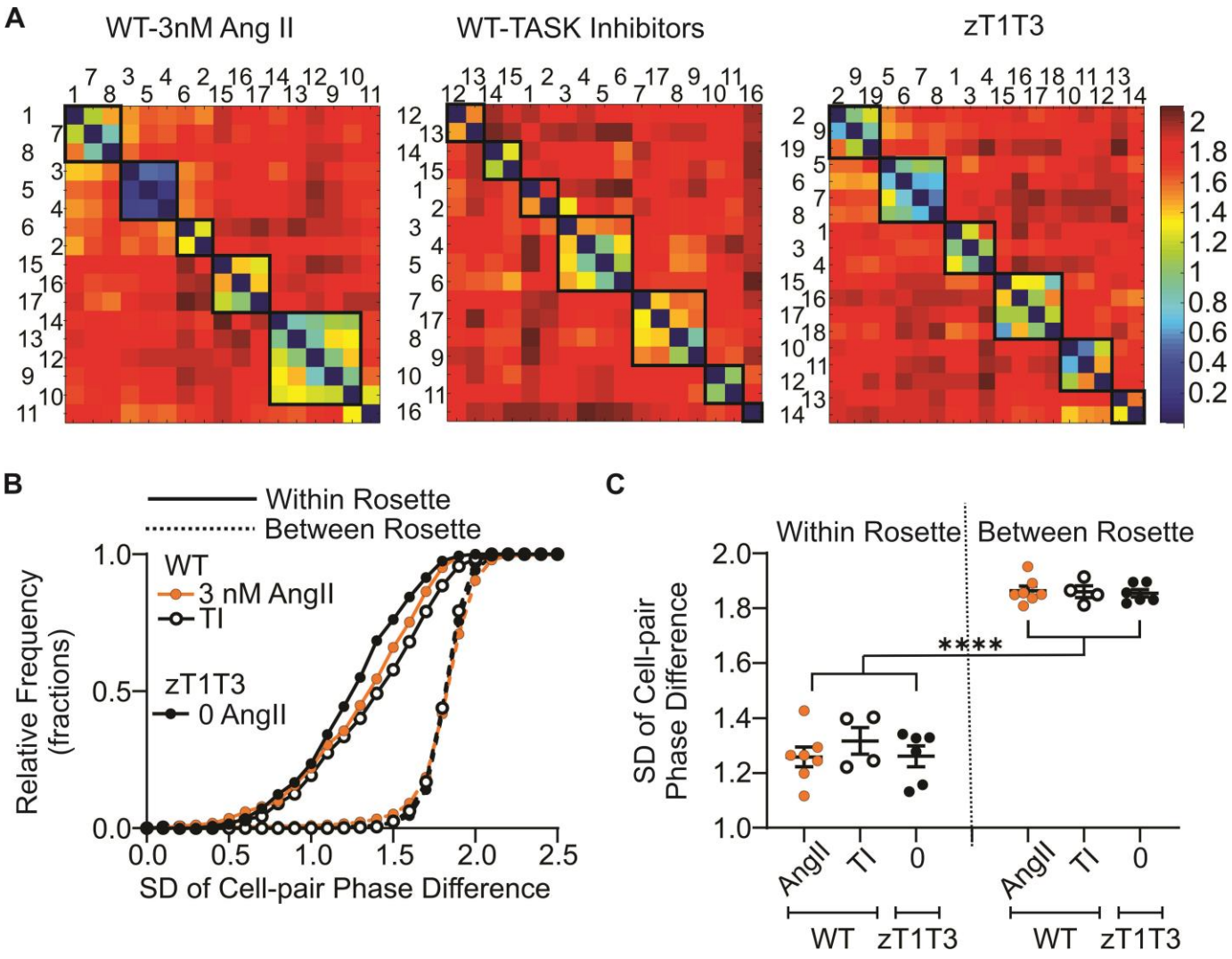

Comparison of AngII-, TASK Inhibitor-, and genetic TASK-LOF-evoked phase-locking. A, Representative matrix plots of pair-wise phase difference SD of calcium spikes in WT slices treated with 3nM AngII (**left**) or TASK inhibitors (**middle**, 200nM A1899 and 200nM PK-THPP), or untreated zG-TASK-LOF (zT1T3) slices (**right**). **B,** Cumulative fraction of cell-cell phase SD and **C,** mean ± SEM of within- and between- rosette phase difference SD from zG-TASK-LOF (black, closed symbols, n=1142 cell-pairs from 6 mice), WT + TASK inhibitors (black, open symbols; n=1079 from 4 mice), and WT + 3nM AngII (orange, closed symbols; n=392 within-, n=1681 cell-pairs from 6 mice). ****P<0.001 as determined by mixed model ANOVA with Bonferroni's multiple comparisons test.